

Original article

Experimental investigation on plugging performance of nanospheres in low-permeability reservoir with bottom water

Meirong Tang¹, Chengwang Wang¹, Xian'an Deng¹, Haifeng Yang², Jun Lu³, Haiyang Yu²*

¹Oil & Gas Technology Research Institute, PetroChina Changqing Oilfield Company, Xi'an 710018, P. R. China

²State Key Laboratory of Petroleum Resources and Prospecting, China University of Petroleum, Beijing 102249, P. R. China

³McDougall School of Petroleum Engineering, The University of Tulsa, Tulsa, 74104, USA

Keywords:

Bottom water reservoir
low permeability
nanospheres
plugging performance
NMR

Cited as:

Tang, M., Wang, C., Deng, X., Yang, H., Lu, J., Yu, H. Experimental investigation on plugging performance of nanospheres in low-permeability reservoir with bottom water. *Advances in Geo-Energy Research*, 2022, 6(2): 95-103.

<https://doi.org/10.46690/ager.2022.02.02>

Abstract:

The oil production rate decreases rapidly after a short period of high yield from acidizing or fracturing in low-permeability reservoirs. In this paper, nanospheres are applied before the fracturing step, which possess the ability to absorb water and expand in the water layer, reducing the flow capacity of bottom water and finally enhancing the oil recovery. The plugging performance is investigated by nanosphere displacement experiments in cores and sand-packs, which explores the plugging effect in the oil layer, the oil-water transition zones, the water layer and the fracturing zones. In addition, a nuclear magnetic resonance experiment is conducted to study the flow mechanism of nanospheres and determine the plugging rates, which can characterize the plugging performance of nanospheres in porous media. The results show that the plugging rate is 85.84% and 78.65% on the water layer and oil-water transition zone, respectively, and 94.36% in the fracturing zone. Meanwhile, the nanospheres cannot plug the oil layer. The formation pressure has a less considerable effect on the plugging performance of nanospheres. The nanospheres have good injectivity, and the intensity variations in small, medium and large pores account for 34.46%, 13.22% and 52.32%, respectively. Overall, this paper explores the feasibility of applying nanospheres for water plugging and enhanced oil recovery.

1. Introduction

Oil and gas remain important energy sources around the world, with the demand increasing year by year (Zhang et al., 2019; Wang et al., 2020; Ajoma et al., 2021; Hosseini et al., 2021). With the depletion of conventional oil and gas resources, the effective development of unconventional reservoirs, such as tight oil and tight gas, is becoming a global propensity (Clark et al., 2018; Wachtmeister and Höök, 2020; Ahmed et al., 2021; Yasin et al., 2021). During the development of unconventional reservoirs in the Ordos Basin, Central China, petroleum engineers have often used fracturing techniques to stimulate the formation (Wang et al., 2019; Li et al., 2021). After the fracturing process, the fracture conductivity of formation is increased, which makes the fluid flow more easily (Ranjbar and Hassanzadeh, 2011; Di et al., 2021;

Memon et al., 2022). However, during fracturing in some tight reservoir with bottom water, the fractures may connect with the bottom water, which results in early water breakthrough or serious water flooding (Alblooshi and Wojtanowicz, 2018; Moghadasi et al., 2019; Akbarifard et al., 2020).

Nanospheres have been employed in profile control and water shutoff in heterogeneous reservoirs for a long time with great results; they could achieve deep profile control by “transporting-plugging-elastic deformation-transporting again-plugging again” (EI-Kaesani et al., 2013; Temizel et al., 2017). The plugging mechanism of nanospheres is mainly divided into physical plugging and elastic plugging. Physical plugging refers to the expansion of nanospheres through water absorption, which could directly plug pores smaller than the diameter of nanoparticle, while elastic plugging refers to the deformation of nanoparticles under pressure, which will be

transported to subsequent pores to continue to play the role of plugging (Eltoum et al., 2021).

Many researchers have conducted laboratory experiments on nanospheres from different aspects. Moghadasi et al. (2019), Eltoum et al. (2021) and Hanafy et al. (2021) tested the effects of injection rate, injection volume and concentration on the plugging performance of nanospheres through core displacement experiments in low permeability reservoirs. Rogachev and Kondrashev (2015), Lenchenkov et al. (2019) and Chen et al. (2020) explored the matching relationship between the pore size and nanosphere size, and studied the influencing factors of plugging through core displacement experiments and microfluidic experiments, in order to reveal the migration and plugging mechanism of nanospheres from the scale of core and pore, respectively. Liang et al. (2019) evaluated the effect of combining nanospheres with other profiling systems through sand-pack displacement experiments. Their results showed that the increase in recovery through the combined technology was greater than that by separate system. Sugar et al. (2021) designed a sophisticated microfluidic chip for profiling experiments to better simulate the real formations, and to assess the nanospheres' plugging effect.

The Nuclear Magnetic Resonance (NMR) technique, which only collects fluid signals (H-signal) and distinguishes different fluids by suppressing the relaxation time, is widely used to analyze rock pore volume, throat size and fluid distribution in oilfield development (David and Douglas, 1988; Saidian and Prasad, 2015; Ghomeshi et al., 2018). Karimi et al. (2018) combined NMR experiments with centrifugation, mercury-pressure capillary pressure, and nitrogen adsorption experiments to investigate the flow and transport mechanisms in shale reservoirs, and clarified the mechanisms contributing to enhanced oil recovery.

This paper presents a method to prevent bottom water intrusion during the development of low-permeability reservoirs with bottom water by injecting nanospheres into the reservoir prior to formation fracturing, in order to create a plug at the bottom water location. The physical properties of nanospheres are firstly investigated by Laser Particle Size Analyzer, and the plugging effect of nanospheres in the matrix and fracturing zone is subsequently evaluated by core and sand-pack displacement experiments. Finally, the injection performance of nanospheres in the matrix is tested by NMR experiments. The above experiments are used to verify the

feasibility of this method.

2. Materials and methods

2.1 Materials

Nanospheres. The nanospheres used in this study were supplied by PetroChina Changqing Oilfield Company and preserved in kerosene. This material can swell in water but not in oil. The median radius of the mother liquid was measured by Nano-Laser Particle Size Analyzer at 124.3 nm, as shown in Fig. 1.

Cores and sand-packs. The cores were taken from the Jurassic Yan 9 and Yan 10 formations in the Ordos Basin, and used for the matrix plugging experiments. Quartz sands with 70/140 mesh were supplied by Jiangsu Tuochuang Scientific Research Instruments Co., Ltd. for the fracture plugging experiments. The parameters of cores and sand-packs are shown in Table 1.

Oil. Crude oil was taken from Jurassic formations in the Ordos Basin, with its composition presented in Fig. 2. It was used for matrix plugging experiments with Core 3. Kerosene (2.310 mPa·s at 25 °C) was adopted for matrix plugging experiments with Core 1. Fluorine oil produced by Minnesota Mining and Manufacturing Company was used in the NMR injectivity experiments.

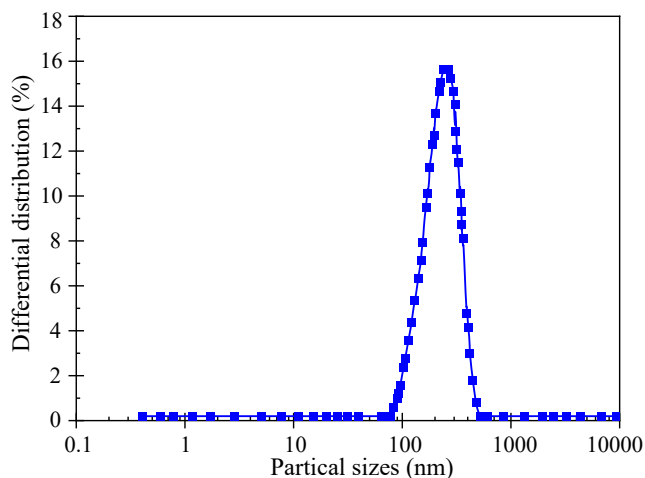


Fig. 1. Particle size distribution of nanospheres in mother solution.

Table 1. Parameters of cores and sand-packs in the corresponding experiments.

Samples	Diameter (cm)	Length (cm)	Porosity	K_g ($\times 10^{-3} \mu m^2$)	Experiments
Core 1	2.508	5.085	0.1659	78.68	Nanospheres matrix plugging
Core 2	2.510	5.085	0.1381	50.952	
Core 3	2.512	5.083	0.1439	27.39	
Core 4	2.468	5.015	0.1587	30.285	NMR injectivity
Sand-pack 1	2.590	51.480	\	13103.73	Nanospheres plugging performance
Sand-pack 2	2.590	51.480	\	12754.08	

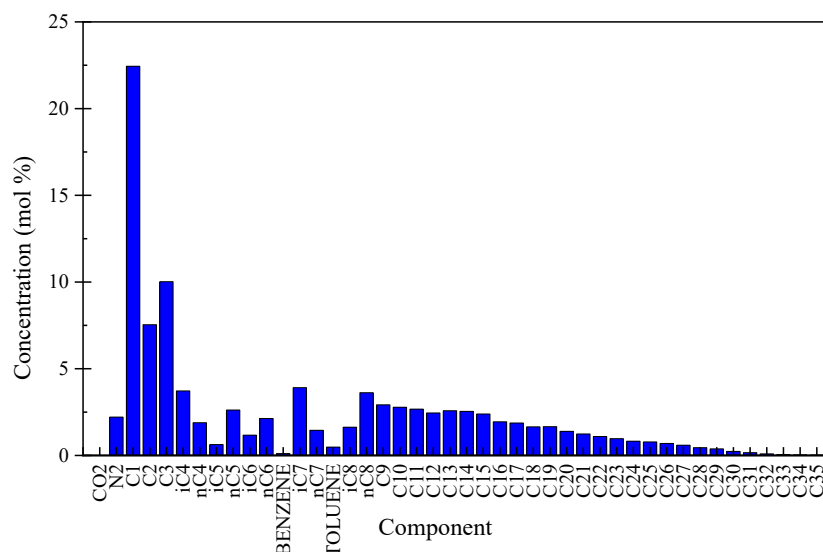


Fig. 2. Composition of the crude oil.

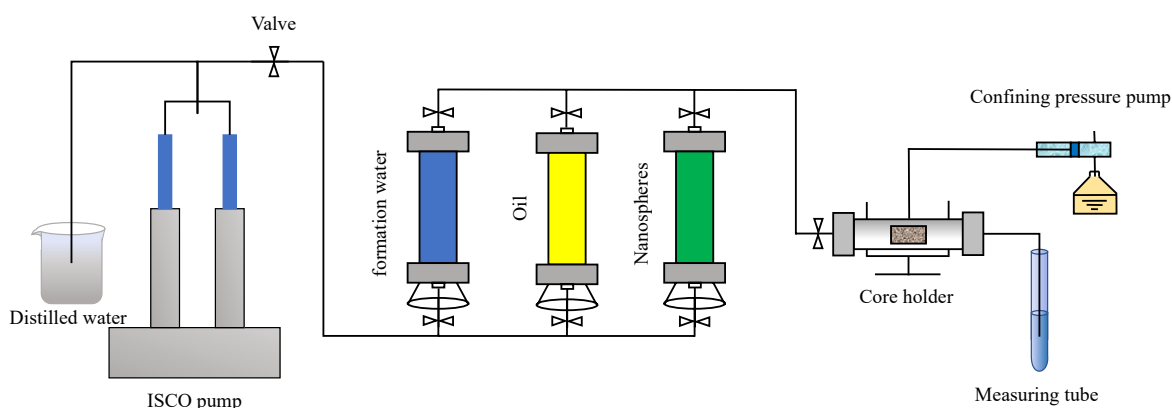


Fig. 3. Schematic diagram of experiments to evaluate nanospheres' matrix plugging performance.

2.2 Experimental methods

Nanospheres particle size distribution test. A Laser Particle Size Analyzer (LSPA) is used in this experiment to determine the particle size distribution of 0.5 wt.% nanosphere solutions in simulated formation water at three different salinities of 0, 20,000 and 80,000 mg/L, with swelling measured at 0, 1, 3, 6 and 8 d to evaluate the swelling effect of the nanospheres, and also to clarify the swelling time of the nanosphere material in subsequent plugging experiments.

Matrix plugging performance experiments. This type of experiments is employed to investigate the plugging performance of nanospheres in matrix by comparing the variation of permeability in cores before and after the injection of nanospheres. Core 1 is saturated with kerosene, Core 2 is saturated with formation water (i.e., 20,000 mg/L KCl solution), and irreducible water state is established in Core 3. The schematic diagram of this experiment is shown in Fig. 3. The experimental equipment includes displacement system (ISCO pump, displacement media, core holder and confining pressure pump) and the measurement system (measuring tubes and pressure transducers). The displacement media contains

formation water, oil and nanosphere solution. The displacement system is used to perform core displacement, and the measurement system is employed to record the experimental data. The prepared cores are subjected to experiments according to the following steps:

Step 1: Kerosene is applied in Core 1, and simulated formation water is used in Core 2 and Core 3 to measure their permeabilities.

Step 2: Nanosphere mother liquid is injected to Core 1, while nanosphere solution (i.e., 0.5 wt.% nanosphere solution in the 20,000 mg/L KCL) is injected to Core 2 and Core 3. Three cores are injected at 3 PV, respectively. The cores are then left to stand for a period of time to allow the nanospheres to reach the expansion limit. The time is determined by the nanosphere particle size distribution test.

Step 3: Step 1 is repeated to obtain the permeability K_{o2} , K_{w2} and K_{w2}' of Core 1, Core 2 and Core 3, respectively, after nanosphere injection.

Step 4: During the experiment, the confining pressure is always 3 MPa higher than the inlet pressure.

Step 5: The plugging rate of the cores in different states is calculated by Eq. (1).

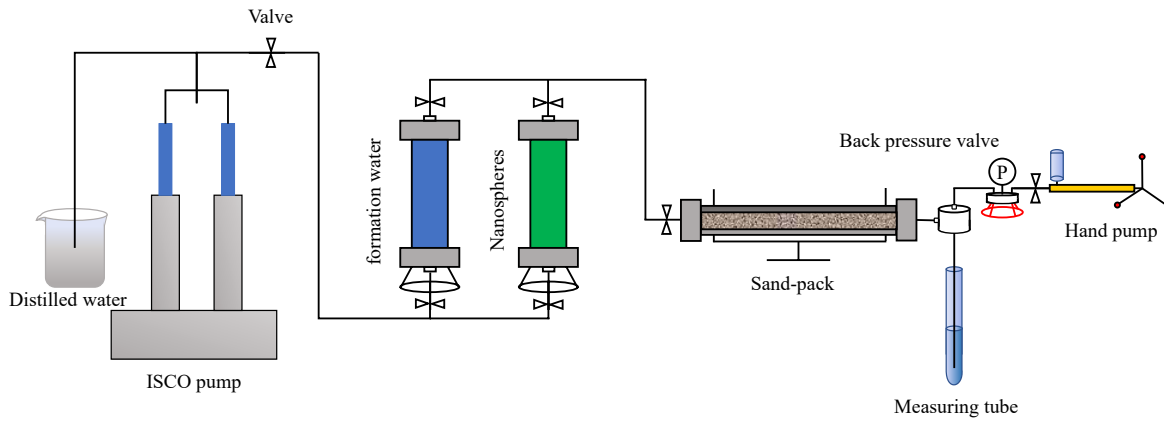


Fig. 4. Schematic diagram of experiments to evaluate nanospheres' fracture plugging performance.

$$\eta = \frac{K_1 - K_2}{K_1} \times 100\% \quad (1)$$

where η represents the plugging rate, %; K_1 represents the permeability obtained at the first time point, $\times 10^{-3} \mu\text{m}^2$; K_2 is the permeability obtained at the second time point, $\times 10^{-3} \mu\text{m}^2$.

Fracture plugging performance experiments. This type of experiments uses sand-packs to simulate the reservoir after fracturing, and the process of bottom water intrusion is simulated by formation water displacement. The fracture plugging performance is investigated by comparing the variation of permeability before and after nanosphere injection. The experimental schematic diagram is shown in Fig. 4. Compared with Fig. 3, the sand-pack replaces the core holder, and a back pressure valve has been added behind it, which regulates the pressure in the sand-pack by a hand pump. The specific steps are performed as follows:

Step 1: Sand-pack 1 and Sand-pack 2 are saturated with formation water (i.e., 20,000 mg/L KCl solution).

Step 2: No back pressure is applied in Sand-pack 1, and 10 MPa back pressure is set in Sand-pack 2.

Step 3: The permeabilities of Sand-pack 1 and Sand-pack 2 are measured by using stimulated formation water.

Step 4: Sand-packs are injected with nanosphere solution (i.e., 0.5 wt.% nanospheres in 20,000 mg/L KCl solution) until the solution flows out of the outlet, and they are left to stand for a period of time to allow the nanospheres to reach their expansion limit.

Step 5: Step 3 is repeated and the permeability of Sand-pack 1 and 2 is measured.

Step 6: The plugging rate of Sand-pack 1 and Sand-pack 2 is calculated by Eq. (1).

Step 7: The pressure at the inlet of sand-packs is increased step-by-step with a step length of 0.2 MPa. Each pressure is applied for a sufficient period of constant pressure. The corresponding pressure is the breakthrough pressure of the water control material, i.e., when there is a uniform and continuous output of water control material at the outlet. Accordingly, the breakthrough pressure gradient is calculated.

Nanosphere NMR injectivity experiments. The laboratory core analysis experiment involving low field nuclear mag-

netic resonance spectroscopy can obtain more accurate and diverse rock information, and provide an effective auxiliary method to study the flow mechanism and EOR performance. The NMR device is used to investigate the distribution of hydrogen signals in cores through establishing the relationship between transverse relaxation time (T_2) and porosity, signal intensity and fluid flow (Pu et al., 2018). Eq. (2) is often used to connect the pore radius and transverse relaxation time:

$$r = \frac{0.735T_2}{C} \quad (2)$$

where r represents pore radius, μm ; T_2 represents NMR transverse relaxation time, ms; and C is the conversion factor. The pore radius distribution curve of the T_2 spectrum conversion fits well with the conventional mercury injection capillary pressure curves when its value is $1.71 \text{ ms}/\mu\text{m}$.

This experiment first divides the pore size of the Jurassic formation by comparing the T_2 spectrum of Core 4 in the saturated simulated formation water, irreducible water and residual oil states. Then, the nanosphere solution is injected at a constant flow rate to investigate the injectivity of the nanospheres into the matrix. Since fluorine oil does not contain the hydrogen element, it does not show up in the T_2 spectrum. In the nanosphere solution, water occupies the majority, and there is only a small percentage of nanospheres, hence the nanosphere solution is close to the intensity of water under the NMR scan. The diagram of the experimental setup is shown in Fig. 5, where an NMR device can be seen around the core holder as opposed to Figs. 3 and 4. This is used for core scan and data analysis. The NMR experimental steps are presented as follows:

Step 1: Core 4 is saturated by simulating formation water after vacuuming, and the core is scanned by NMR equipment to obtain T_2 spectrum under the 100% water saturation.

Step 2: The irreducible water state is obtained in Core 4 by using fluorine oil to displace the 100% saturated water. Afterwards, the NMR equipment is applied to scan this core for the T_2 spectrum.

Step 3: The irreducible water state is obtained in Core 4 by using formation water and then scanned to obtain the T_2 spectrum in the residual oil state.

Step 4: Core 4 in the residual oil state is placed in the NMR

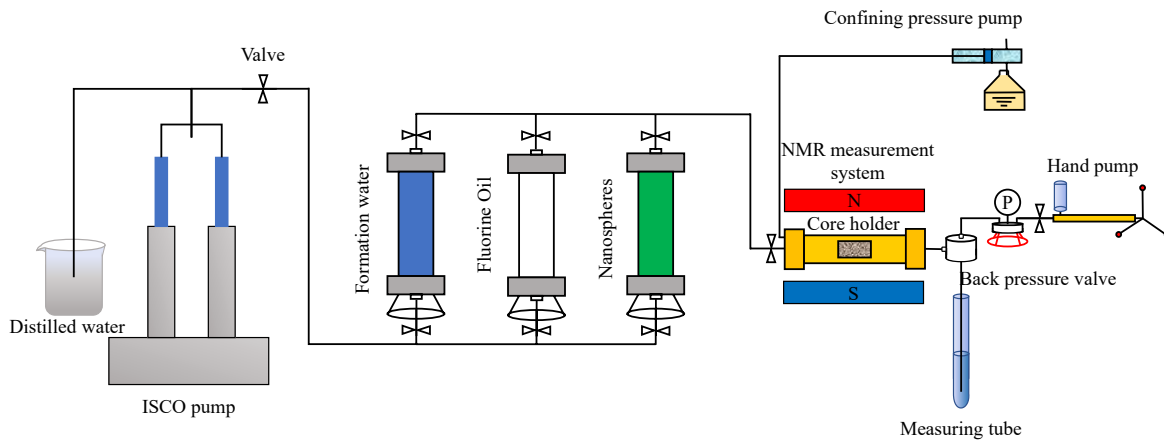


Fig. 5. Schematic diagram of nanosphere NMR injectivity experiments.

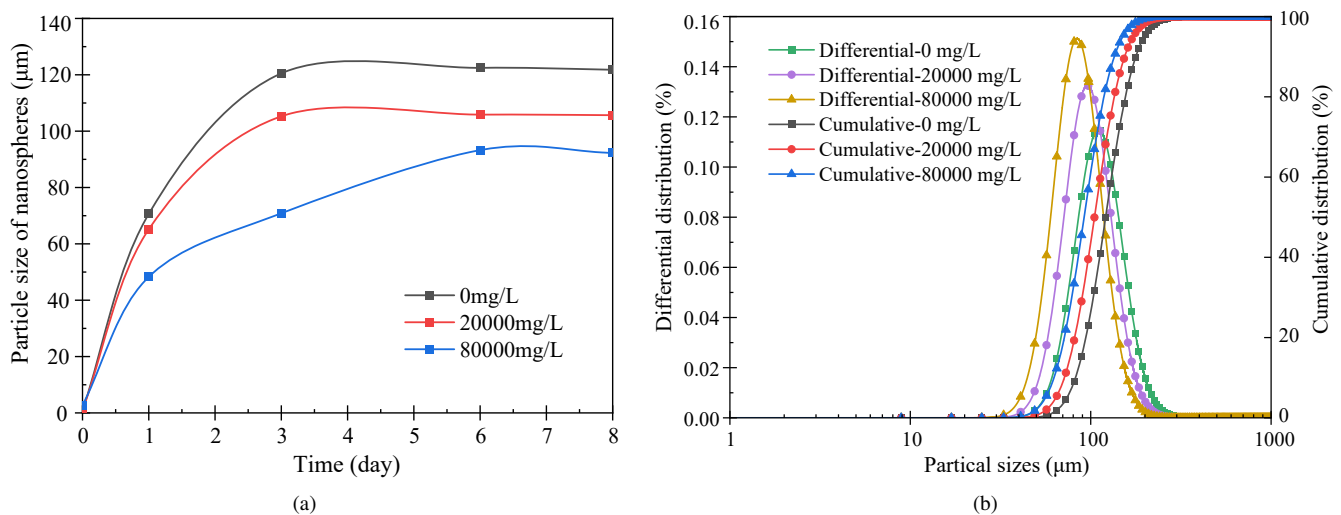


Fig. 6. Particle size of nanospheres tested by LPSA. (a) Particle sizes change in water with increasing salinity during swelling time. (b) Particle size distribution of nanospheres after reaching swelling equilibrium.

experiment. A back pressure of 0.5 MPa is applied and the nanosphere solution is injected at a flow rate of 0.05 mL/min. The online NMR scanning is performed for every 0.25 PV injected, with an injection volume of 3 PV.

Step 5: During the experiment, the confining pressure is always 3 MPa higher than the inlet pressure.

3. Results and discussion

3.1 Nanospheres particle size distribution

The size of nanospheres is their median size measured by LPSA (Fig. 6). The particle sizes of nanospheres are 121.8, 105.7 and 92.3 μm when the particles reached swelling equilibrium in simulated formation water at 0, 20,000 and 80,000 mg/L mineralization levels, respectively (Table 2). A Leica microscope was used to observe the nanospheres solution under 20,000 mg/L simulated formation water (0 d). It was shown that the diameter of the nanoparticles expands and they agglomerate rapidly in water (Fig. 7).

The results showed that particle size increases from nano

Table 2. Particle size and swelling time when nanospheres reach swelling equilibrium.

Salinity (mg/L)	Particle sizes (μm)	Swelling time (d)
0	121.8	3
20,000	105.7	3
80,000	92.3	6

-scale to microscale after absorbing water. The nanospheres swell from 124.3 nm to 0.856, 0.932 and 2.677 μm in 0, 20,000 and 80,000 mg/L formation water, respectively. Three days were needed to reach the swelling equilibrium under the conditions of 0 and 20,000 mg/L formation water, while about 5-6 days were required to reach swelling equilibrium in 80,000 mg/L formation water due to the salinity effect.

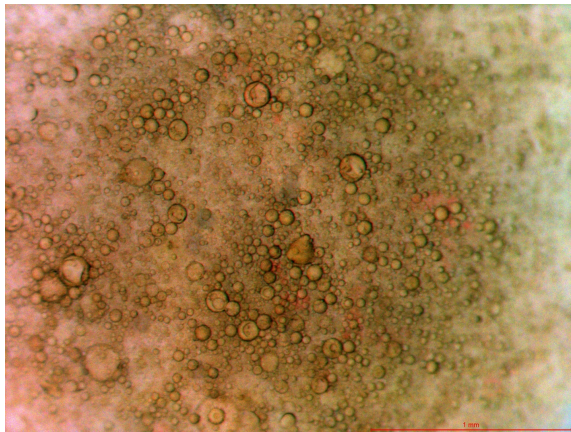
The findings revealed that the particle size of nanospheres in the fresh nanosphere solution increases with the rising salinity of the formation water, and decreases when reaching swelling equilibrium. However, the time needed to reach the

Table 3. Result of nanospheres matrix plugging performance experiments.

Sample	$K_1 (\times 10^{-3} \mu\text{m}^2)$	$K_2 (\times 10^{-3} \mu\text{m}^2)$	η (%)	Conditions
Core 1	42.080	42.080	0	Oil layer
Core 2	9.996	1.415	85.84	Water layer
Core 3	0.248	0.053	78.65	Oil-water transition zone

Table 4. Result of nanosphere fracture plugging performance experiments.

Sample	$K_1 (\times 10^{-3} \mu\text{m}^2)$	$K_2 (\times 10^{-3} \mu\text{m}^2)$	η (%)	P_b (MPa)	G_b (MPa/m)
Sand-pack 1	13103.73	739.54	94.36	1.2-1.4	2.33-2.72
Sand-pack 2	12754.08	687.44	94.61	1.2-1.4	2.33-2.72

**Fig. 7.** Nanosphere patterns observed under Leica microscope.

swelling limit increases in higher salinity (80,000 mg/L) formation water. Therefore, the compatibility of the nanospheres should be considered in field application.

3.2 Nanospheres' matrix plugging performance

Plugging rate is an important indicator to evaluate the water control performance of nanospheres. In this experiment, the result for Core 1 simulated the process of nanosphere mother solution entering the oil formation. It could be used to evaluate the plugging effect of nanospheres, and clarify the damage of nanospheres in oil formation by calculating the plugging rate. The experiment involving Core 2 simulated the process of nanosphere solution entering the water formation, which revealed the plugging effect of nanospheres in the water formation by calculating the plugging rate of Core 2. The experiment involving Core 3 simulated the process of nanospheres entering the oil-water transition zone ($S_w = 45.23\%$), which revealed the plugging performance of nanospheres in the oil-water transition zone by calculating the plugging rate of Core 3. The results are shown in Table 3.

The results indicated that the plugging rate in the oil formation, in the water formation, and in the oil-water transition zone was 0, 85.84%, and 78.65%, respectively. This illustrated that nanospheres firstly enter the oil formation, then the oil-water transition zone, and finally the water formation during the injection process from the wellbore to the formation. The

nanospheres would form a baffle at the location of the water formation and the oil-water transition zone after swelling in the formation for 3 days, which effectively prevents the intrusion of bottom water during development. Flowable nanospheres in the reservoir will flow out with the extracted oil, and the trapped nanospheres will form another plug as the oil-water transition zone level rises during development.

3.3 Nanospheres fracture plugging performance

In this experiment, the sand-packs were used to simulate the fractured zone, and the plugging rate, breakthrough pressure (P_b) and breakthrough pressure gradient (G_b) were measured to evaluate the plugging effect of nanospheres in fractures. The plugging rates of nanospheres under different pressures were investigated by applying different back pressures on sand-packs. The results are shown in Table 4.

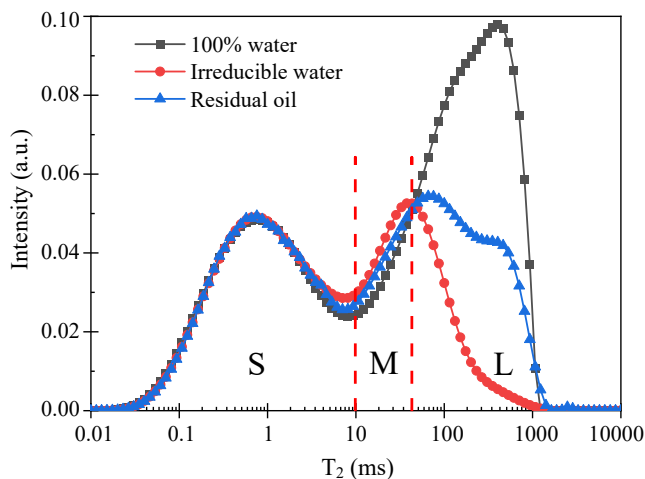
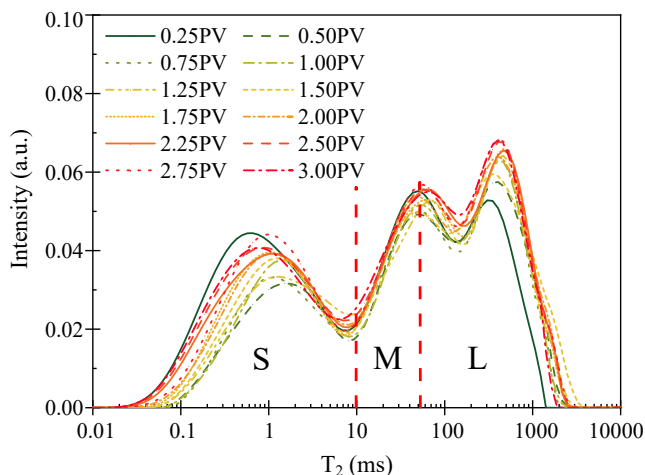
Sand-pack 1 and Sand-pack 2 were filled in the same way, and they could be considered to have almost the same initial permeability. The plugging rates for Sand-pack 1 and Sand-pack 2 were 94.36% and 94.61%, respectively, with the same breakthrough pressures between 1.2 and 1.4 MPa and the same breakthrough pressure gradient of 2.33-2.72 MPa/m. The results showed that the change of formation pressure has negligible effect on the plugging performance of the nanospheres as the well is developed. The pressure keeps decreasing under the condition that the formation energy is not replenished when the nanospheres in the matrix cannot effectively plug the intrusion of bottom water. The bottom water intrudes into the fractured zone because the nanospheres can absorb water. Then, it expands in the bottom water intrusion zone to form a second baffle. In the late stage of development, the plugging performance of the nanospheres is not diminished when formation energy is supplied and the formation pressure rises.

3.4 Flow mechanism of nanospheres by NMR

The pores of the Jurassic cores were classified according to the T_2 spectrum (Fig. 8) of the cores at 100% water, irreducible water and residual oil, respectively. The results are shown in Table 5. The cores were then injected with the nanosphere solution, and online NMR scans were performed to obtain the T_2 spectrum (Fig. 9) during the injection process. The injection

Table 5. The basis and results of pores division.

Parameters	Small pore	Medium pore	Large pore
T_2 (ms)	<10	10-50	>50
Pores radius (μm)	<4.3	4.3-21.5	>21.5
Pores percentage (%)	34.46	13.22	52.32

**Fig. 8.** T_2 spectrum at the conditions of 100% water, irreducible water and residual oil.**Fig. 9.** T_2 spectrum during nanosphere injection.

capacity of the nanospheres was evaluated by analyzing the intensity variations of the large, medium and small pores during the injection process (Figs. 10 and 11). In contrast to previous researches, this paper investigated the flow mechanism of nanospheres in low-permeability cores by comparing the intensity variation of different pores.

As Core 4 is a low-permeability core, its T_2 spectrum has an obvious double-peaked structure (Fig. 8). This study takes the scope between the two peaks of the T_2 spectrum of Core 4 (i.e., T_2 of 10 ms and pore radius of 4.3 μm) to divide small and medium pores. However, the wave crest at the right

side decreases and moves to the left during the 100% water to residual oil state. The spectrum changes little at T_2 less than 50 ms, while the change is obvious at the opposite end, indicating that pores greater than 21.5 μm in Core 4 are easily used in the process of water displacing oil or oil displacing water. Therefore, the transverse relaxation time of 50 ms, corresponding to a pore radius of 21.5 μm , could be used as the dividing line between the medium and large pores. The basis of pore division is shown in Table 5. The T_2 spectrum of 100% water reflects the pore structure of the core. According to the basis, the result of pores division is that the small pores take up 34.51%, the medium pores amount to 13.17%, and the large pores consist 52.32% (Table 5).

The results of online NMR experiments of Core 4 nanosphere injection are shown in Fig. 9. The small pores' crest moves to the left (i.e., the direction of decreasing relaxation time), indicating that the nanospheres enter smaller pores as the experiment progresses. The increasing intensity in the medium and large pores indicates that the residual oil is being displaced by the nanosphere solution, and the nanospheres continue to enter the medium and large pores.

In the T_2 spectrum, the area enclosed by the curve could characterize the intensity of the hydrogen signal. The peak areas of the small, medium and large pores in the online NMR T_2 spectrum were quantified. In the small pores (Fig. 10(a)), the total intensity of the nanospheres show a decreasing trend at 0.5 PV injection, followed by an increasing total intensity during the injection of 0.5 to 2.5 PV, and the intensity of the hydrogen signal gradually flattens out after 2.5 PV of nanosphere injection. In the medium pores (Fig. 10(b)), the trend of total intensity is basically the same as that in the small pores, but the magnitude of intensity variation is smaller. In the large pores (Fig. 10(c)), the overall trend in total intensity is increasing, and the intensity of the hydrogen signal flattens out after 2.5 PV injections. During the injection of 0.5 PV nanospheres, the total intensity in the small and medium pores decrease and the intensity in the large pores increase, which indicates that some of the fluorine oil in the large pores enter the small and medium pores at this time. After the injection of 0.5 PV, the total intensity in the different pores show an upward trend, which indicates that it the nanospheres continuously enter the large, medium and small pores.

To better investigate the injectability of the nanospheres in the matrix, the T_2 spectrums of initial state (i.e., residual oil), 0.5 PV of nanosphere injection and 3.0 PV of nanosphere injection were analyzed for comparison (Fig. 11). It demonstrated that the total intensity of the small and medium pores reaches a minimum value when 0.5 PV of nanospheres are injected, and then the total intensity increases continuously (Figs. 10(a) and 10(b)). The increasing after 0.5 PV injection is caused by nanosphere solution entering the pores. Therefore, this paper used the T_2 spectrum of 0.5 and 3.0 PV nanospheres injection to analyze the flow mechanisms in small and middle pores. The total intensity in the large pores was increasing (Fig. 10(c)), so this paper compared the total intensity in the initial state with the end state of the experiment (i.e., 3.0 PV of nanospheres injection) to investigate the flow mechanisms in large pores. The intensity variations in the small, medium

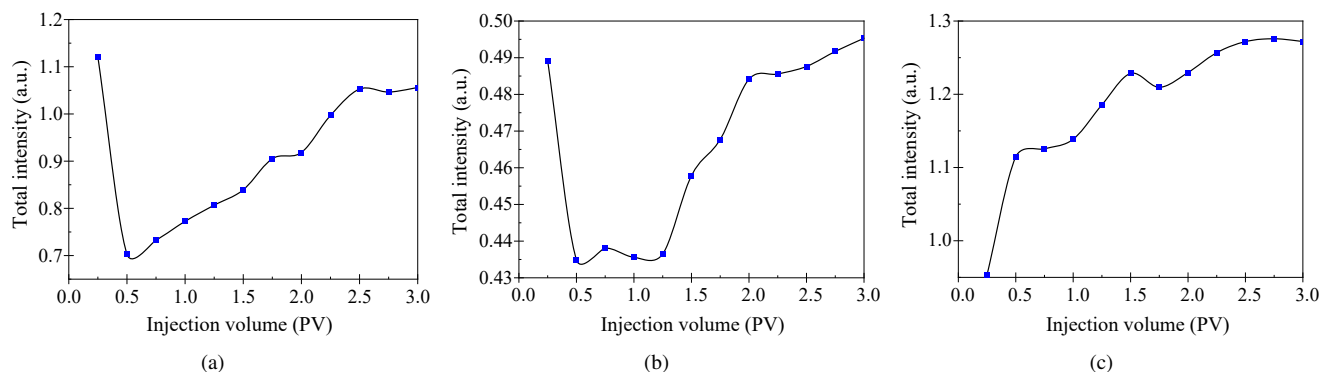


Fig. 10. Variations of total intensity during the injection. (a) Variations in the small pores. (b) Variations in the medium pores. (c) Variations in the large pores.

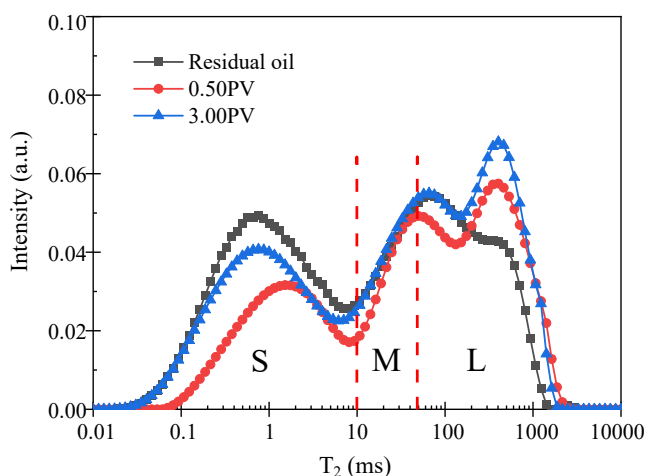


Fig. 11. T_2 spectrum at the conditions of residual oil, injection of 0.50 PV nanospheres and injection of 3.00 PV nanospheres.

Table 6. The variations of intensity in the small, medium and large pores.

Variations	Small pore	Medium pore	Large pore
Intensity	0.376	0.08	0.298
Percentage (%)	49.87	10.61	39.52

and large pores were 0.376, 0.08 and 0.298, accounting for 49.87%, 10.61% and 39.52% of the total intensity variation, respectively (Table 6).

4. Conclusions

In this paper, nanospheres were employed to plug the bottom water and enhance oil recovery in low-permeability reservoirs. Different experiments were conducted to investigate the plugging mechanism. The main findings are as follows:

- 1) The nanospheres expand rapidly, and the clustering phenomenon occurs when they combine with water. There is a weaker effect of nanospheres on swelling at low salinity; formation water salinity can inhibit the nanospheres' swelling and clustering to a certain extent.

- 2) The plugging rates of nanospheres in the oil layer, water layer and oil-water transition zones are 0, 85.84% and 78.65%, respectively. Therefore, the nanospheres do not swell or plug when they come in contact with oil, but they can prevent the bottom water intrusion by forming a bulkhead in the water layer and the oil-water transition zone.
- 3) The plugging performance of nanospheres in the fractured zone is not affected by pressure changes. There is only 0.25% change in the plugging rate at 0.1 and 10 MPa conditions. When bottom water intrudes into the fractured zone, the nanospheres in the fractures will swell and have a plugging effect.
- 4) The online NMR experimental results demonstrate that the initial 0.5 PV of nanospheres play a profile control role. The intensity variations in small, medium and large pores account for 34.46%, 13.22% and 52.32% of the total intensity, respectively, which indicates that the nanospheres have good injectivity into pores.

Acknowledgement

This work was financially supported by the National Natural Science Foundation of China (Nos. 51874317, 52074317), the Science Foundation of China University of Petroleum Beijing (No. 2462020YXZZ028), and the Strategic Cooperation Technology Projects of CNPC and CUPB (No. ZLZX2020-02-04-04). Special thanks are given to Changqing Oilfield for providing reservoir cores, crude oil, nanospheres, and other important data.

Conflict of interest

The authors declare no competing interest.

Open Access This article is distributed under the terms and conditions of the Creative Commons Attribution (CC BY-NC-ND) license, which permits unrestricted use, distribution, and reproduction in any medium, provided the original work is properly cited.

References

Ahamed, M. A. A., Perera, M. S. A., Elsworth, D., et al. Effective application of proppants during the hydraulic fracturing of coal seam gas reservoirs: Implications from

- laboratory testings of propped and unpropped coal fractures. *Fuel*, 2021, 304: 121394.
- Ajoma, E., Saira, Sungkachart, T., et al. Effect of miscibility and injection rate on water-saturated CO₂ Injection. *Energy*, 2021, 217: 119391.
- Akbarifard, M. G., Azdarpour, A., Aboosadi, Z. A., et al. Numerical simulation of water production process and spontaneous imbibition in a fractured gas reservoir—A case study on homa gas field. *Journal of Natural Gas Science and Engineering*, 2020, 83: 103603.
- Alblooshi, Y. A., Wojtanowicz, A. K. Dynamic water control in naturally fractured bottom water-drive reservoirs via downhole water sink well deployment: First experimental study. Paper SEG-2018-35 Presented at SEG/AAPG/EAGE/SPE Research and Development Petroleum Conference and Exhibition, Abu Dhabi, UAE, 9-10 May, 2018.
- Chen, X., Li, Y., Liu, Z., et al. Core- and pore-scale investigation on the migration and plugging of polymer microspheres in a heterogeneous porous media. *Journal of Petroleum Science and Engineering*, 2020, 195: 107636.
- Clark, J. A., Santiso, E. E. Carbon sequestration through CO₂ foam-enhanced oil recovery: A green chemistry perspective. *Engineering*, 2018, 4(3): 336-342.
- David, P. G., Douglas, M. S. A NMR technique for the analysis of pore structure: Determination of continuous pore size distributions. *Journal of Colloid and Interface Science*, 1988, 122(1): 143-153.
- Di, S., Cheng, S., Bai, W., et al. Dynamic fracture propagation mechanism and application tight oil reservoir. *Chinese Journal of Theoretical and Applied Mechanics*, 2021, 53(8): 2141-2155. (in Chinese)
- EI-Kaesani, K. S., AI-Muntasheri, G. A., Hussein, I. A. Polymer systems for water shutoff and profile modification: A review over the last decade. *SPE Journal*, 2013, 19(1): 135-149.
- Eltoum, H., Yang, Y., Hou, J. The effect of nanoparticles on reservoir wettability alteration: A critical review. *Petroleum Science*, 2021, 18: 136-153.
- Ghomeshi, S., Kryuchkov, S., Kantzas, A. An investigation into the effects of pore connectivity on T₂ NMR relaxation. *Journal of Magnetic Resonance*, 2018, 289: 79-91.
- Hanafy, A., Najem, F., Nasr-EI-Din, H. A. Effect of nanoparticle shape on viscoelastic surfactant performance at high temperatures. *SPE Journal*, 2021, 26(3): 1436-1454.
- Hosseini, S. H., Shakouri, G. H., Kazemi, A. Oil price future regarding unconventional oil production and its near-term deployment: A system dynamics approach. *Energy*, 2021, 222: 119878.
- Karimi, S., Kazemi, H. Characterizing pores and pore-scale flow properties in middle bakken cores. *SPE Journal*, 2018, 23(4): 1343-1358.
- Lenchenkov, N. S., Slob, M., Glasbergen, G., et al. Propagation of polymer nanospheres in outcrop cores. *SPE Journal*, 2019, 24(6): 2776-2792.
- Li, G., Liu, G., Hou Y., et al. Optimization method of favorable lithofacies and fracturing parameter for continental shale oil. *Acta Petrolei Sinica*, 2021, 42(11): 1405-1416. (in Chinese)
- Liang, S., Hu, S., Li, J., et al. Study on EOR method in offshore oilfield: Combination of polymer microspheres flooding and nitrogen foam flooding. *Journal of Petroleum Science and Engineering*, 2019, 178: 629-639.
- Memon, S., Feng, R., Ali, M., et al. Supercritical CO₂-Shale interaction induced natural fracture closure: Implications for scCO₂ hydraulic fracturing in shales. *Fuel*, 2022, 313: 122682.
- Moghadasi, R., Rostami, A., Hemmati-Sarapardeh, A. Application of nanofluids for treating fines migration during hydraulic fracturing: Experimental study and mechanistic understanding. *Advances in Geo-Energy Research*, 2019, 3(2): 198-206.
- Pu, W., Zhao, S., Wang, S., et al. Investigation into the migration of polymer microspheres (PMs) in porous media: Implications for profile control and oil displacement. *Colloids and Surfaces A: Physicochemical and Engineering Aspects*, 2018, 540: 265-275.
- Ranjbar, E., Hassanzadeh, H. Matrix–fracture transfer shape factor for modeling flow of a compressible fluid in dual-porosity media. *Advances in Water Resource*, 2011, 34(5): 627-639.
- Rogachev, M., Kondrashev, A. Experiments of fluid diversion ability of a new waterproofing polymer solution. *Petroleum Exploration and Development*, 2015, 42(4): 554-559.
- Saidian, M., Prasad, M. Effect of mineralogy on nuclear magnetic resonance surface relaxivity: A case study of Middle Bakken and Three Forks formations. *Fuel*, 2015, 161: 197-206
- Sugar, A., Torrealba, V., Buttner, U., et al. Assessment of polymer-induced clogging using microfluidics. *SPE Journal*, 2021, 26(6): 3793-3804.
- Temizel, C., Putra, D., Zhang, M., et al. Smart nanoparticles for conformance improvement in waterflooding. Paper SPE 186889 Presented at the SPE/IATMI Asia Pacific Oil & Gas Conference and Exhibition, Jakarta, Indonesia, 17-19 October, 2017.
- Wachtmeister, H., Höök, M. Investment and production dynamics of conventional oil and unconventional tight oil: Implications for oil markets and climate strategies. *Energy and Climate Change*, 2020, 1: 100010.
- Wang, Y., Ayala, L. F. Explicit Determination of reserves for variable bottom-hole pressure conditions in gas well decline analysis. *SPE Journal*, 2020, 25(1): 369-390.
- Wang, Y., Cheng, S., Zhang, K., et al. A comprehensive work flow to characterize waterflood-induced fracture by integrating real-time monitoring, formation test, and dynamic production analysis applied to Changqing Oilfield, China. *SPE Reservoir Evaluation and Engineering*, 2019, 22(2): 692-708.
- Yasin, Q., Sohail, G. M., Liu, K. -Y., et al. Study on brittleness templates for shale gas reservoirs-A case study of Longmaxi shale in Sichuan Basin, southern China. *Petroleum Science*, 2021, 18(5): 1370-1389.
- Zhang, T., Li, Y., Sun, S. Phase equilibrium calculations in shale gas reservoirs. *Capillarity*, 2019, 2(1): 8-16.